AIP | Applied Physics Letters

Effect of the energy dependence of the carrier scattering time on the thermoelectric power factor of quantum wells and nanowires

Jane E. Cornett and Oded Rabin

Citation: Appl. Phys. Lett. **100**, 242106 (2012); doi: 10.1063/1.4729381
View online: http://dx.doi.org/10.1063/1.4729381
View Table of Contents: http://apl.aip.org/resource/1/APPLAB/v100/i24
Published by the American Institute of Physics.

Effect of the energy dependence of the carrier scattering time on the thermoelectric power factor of quantum wells and nanowires

Jane E. Cornett[1] and Oded Rabin[1,2,a)]
[1]*Department of Materials Science and Engineering, University of Maryland, College Park, Maryland 20742, USA*
[2]*Institute for Research in Electronics and Applied Physics, University of Maryland, College Park, Maryland 20742, USA*

(Received 20 March 2012; accepted 18 May 2012; published online 13 June 2012)

The size-dependence of the thermoelectric power factor of thin-films and nanowires is theoretically investigated from the electric quantum limit (EQL) to the bulk-like regime. Different functional forms of the energy-dependent relaxation time $\tau(E)$ are incorporated in the model to account for carrier scattering mechanisms typical in semiconductor nanostructures. The calculations show that the steeper the increase in the relaxation time with carrier energy, the higher the power factor-to-average scattering time ratio, $PF/\langle\tau\rangle$, confirming the benefits of the preferential scattering of low-energy carriers to thermoelectric performance. However, outside the EQL, the power factor values are lower in the low-dimensional structures than in their three-dimensional counterparts. Thus, the power factor is more readily improved by modifications of the scattering rates than by quantization of the energy states. © *2012 American Institute of Physics*. [http://dx.doi.org/10.1063/1.4729381]

The efficiency of a thermoelectric material is determined by its figure-of-merit, $ZT = \sigma S^2 T/\kappa$, where σ is the electrical conductivity, S is the Seebeck coefficient, T is the absolute temperature, and κ is the thermal conductivity. Large ZT values are often difficult to achieve because the various transport properties involved are related in unfavorable ways (e.g., the Wiedemann-Franz law). Approaches leading to improvements in ZT have for the most part focused either on (a) suppressing phonon transport, reducing the lattice thermal conductivity,[1–3] or (b) enhancing the electronic transport properties via carrier filtering,[4,5] resonant level doping,[6,7] and band structure engineering.[8,9] Low-dimensional and nanostructured thermoelectrics present a possible route for utilizing both effects.[10,11]

The prediction of high ZT values in nanowires and thin films is credited to Hicks and Dresselhaus. Using the constant relaxation time approximation (CRTA), they obtained a monotonic increase in the thermoelectric power factor ($PF = \sigma S^2$) with increasing confinement.[12,13] This result is only valid in the electric quantum limit, where a single electron energy subband contributes to charge transport. Subsequent modifications of the model sought to account for carrier scattering by acoustic phonons, polar optical phonons, ionized impurities, and heterostructure interfaces in order to more adequately represent realistic materials systems at or near the electric quantum limit.[14–18] The results of these models depend on the energy- and size-dependence of the scattering rates and may deviate substantially from those of the CRTA model.

We have previously developed a model for the thermoelectric transport properties of nanowires and quantum wells suitable for systems falling outside the electric quantum limit.[19,20] We have reported that for most of the size range investigated, the nanoscale PF is lower than the bulk PF and increases (up to the bulk value) as the size increases. This result was demonstrated to be universal regardless of effective mass, mobility, temperature or dimension with the assumption of a single, parabolic dispersion Fermi pocket, an infinite potential well, and a constant carrier relaxation time.[20] As with the models developed for the electric quantum limit, the applicability of these CRTA results to real semiconductor systems requires further analysis of the power factor in the context of various scattering mechanisms.

In the present work, we address the size-dependence of the thermoelectric power factor of nanoscale systems for which the scattering time varies with carrier energy. We report that the thermoelectric PF of quantum wells and nanowires exhibits qualitatively the same size-dependence regardless of the particular scattering mechanism (and corresponding energy-dependence) that dominates charge-carrier transport.

The lowest 300 subband energies for each quantum well of thickness a (nanowire of radius r) were determined by solving the Schrödinger equation for electrons confined in a one-(two-) dimensional infinite potential well.[21] We assume a wide bandgap semiconductor, such that a single majority carrier is present. The majority carriers, taken to be electrons, are characterized by an isotropic effective mass $m^* = 0.013m_0$, where m_0 is the free electron mass. Transport property calculations were performed by solving the Boltzmann transport equation as a function of Fermi energy and film thickness a (nanowire radius r) under the non-uniform relaxation time approximation.[12,13] Analogous calculations were done for bulk.[22] For each well thickness and nanowire radius, the PF values reported have been optimized with respect to Fermi energy. In contrast to the CRTA approach, the carrier scattering rate is chosen to have the form

$$\tau^{-1}(E) = \sum_i \tau_i{}^{-1}(E) = \sum_i \left(C_i \cdot (E/k_B T)^{p_i}\right)^{-1}, \quad (1)$$

a)Author to whom correspondence should be addressed. Electronic mail: oded@umd.edu.

following Matthiessen's rule. In Eq. (1), τ is the electron relaxation time, C_i is a constant coefficient (with units of time) for scattering mechanism i, E is the carrier energy relative to the conduction band edge, k_B is the Boltzmann constant, and p_i defines the exponential energy-dependence of the scattering time. This model excludes a possible size-dependence of the scattering time, which may be significant at sizes on the order of the carrier mean free path.[16] The range of p_i values investigated (-0.8 to 1.5) includes those frequently used in modeling various scattering processes. For example, the scattering rate may be proportional to the density of final states; for bulk this corresponds to $p=-0.5$, for quantum wells to $p=0$ and nanowires to $p=0.5$.[23] This model is often associated with scattering off of acoustic phonons.[24] Another example is a system in which the scattering rate is proportional to the carrier velocity. For the parabolic band assumed here, this corresponds to $p=-0.5$ for all dimensions.[23] The range of energy-dependences studied also includes those associated with scattering off of ionized impurities[25] and polar optical phonons,[26] though the equations frequently used to model the relaxation times for these mechanisms cannot be written explicitly in terms of a single exponent p_i.

We first focus on a system in which the scattering time can be expressed with a single power-dependence on energy, i.e., $\tau = C\cdot(E/k_BT)^p$. There are two independent parameters: (1) the exponent p, which controls the energy-dependence of the scattering time, and (2) the coefficient C, which determines the magnitude of the scattering time. In this work, we focus on the former parameter as, in general, an increase in scattering time corresponds to an increase in the values of the thermoelectric transport properties, including the electrical conductivity and the power factor. To eliminate the effect of changing the *magnitude* of the scattering time, the coefficient C is chosen such that for each p,$\langle\tau\rangle$, the average scattering time defined as

$$\langle\tau\rangle = \frac{m^*}{e^2}\frac{\sigma}{n} = \frac{\int_0^\infty \tau(E)\cdot \mathrm{DOS}(E)\cdot f(E)dE}{\int_0^\infty \mathrm{DOS}(E)\cdot f(E)dE}, \qquad (2)$$

is equal to the scattering time assumed under the constant relaxation time approximation (i.e., $\langle\tau\rangle=\tau_{CRTA}$, where $\tau_{CRTA}=5.18\cdot10^{-13}$s—the reported value for n-type InSb (Refs. 27 and 28)). In Eq. (2), DOS$(E)dE$ is the electron density-of-states in m^{-3} and $f(E)$ is the Fermi-Dirac distribution. It can be shown that multiplication of the PF by the factor $(\tau_{CRTA}/\langle\tau\rangle)$ is equivalent to evaluating the power factor of a system with C chosen such that the magnitude of $\langle\tau\rangle=\tau_{CRTA}$.

Optimized $PF_{2D}\cdot(\tau_{CRTA}/\langle\tau_{2D}\rangle)$ values for quantum wells are shown as a function of well thickness for p values between -0.8 and 1.5 in Fig. 1(a). For each p value, $PF_{2D}\cdot(\tau_{CRTA}/\langle\tau_{2D}\rangle)$ shows a non-monotonic dependence on a—decreasing down to a minimum, then increasing asymptotically to the bulk value for large thicknesses. On the other hand, for a given a, $PF_{2D}\cdot(\tau_{CRTA}/\langle\tau_{2D}\rangle)$ increases monotonically with p. The bulk value, $PF_{3D}\cdot(\tau_{CRTA}/\langle\tau_{3D}\rangle)$, also increases with p (Fig. 1(b)).

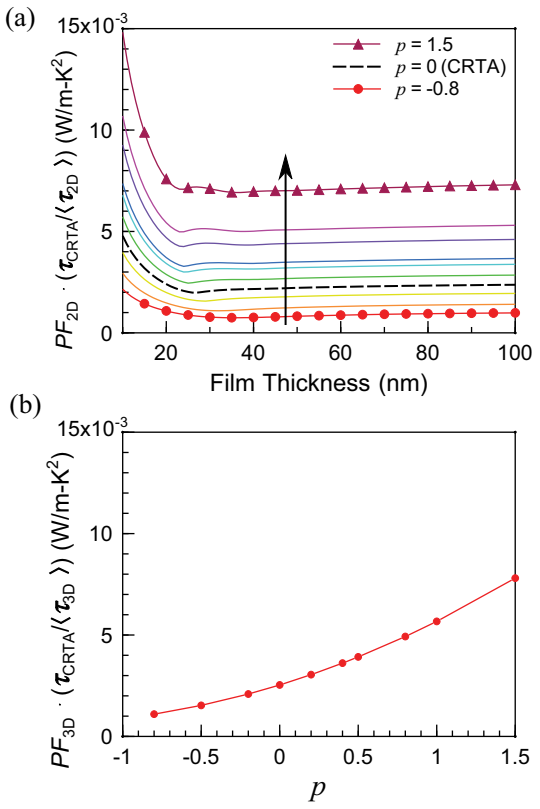

FIG. 1. (a) $PF_{2D}\cdot(\tau_{CRTA}/\langle\tau_{2D}\rangle)$ as a function of film thickness for the range of p values investigated. The black arrow indicates the trend of increasing p. Starting with the bottom curve, the values of p are -0.8, -0.5, -0.2, 0 (CRTA), 0.2, 0.4, 0.5, 0.8, 1, and 1.5. (b) Bulk $PF_{3D}\cdot(\tau_{CRTA}/\langle\tau_{3D}\rangle)$ values as a function of p.

The optimized $PF_{2D}\cdot(\tau_{CRTA}/\langle\tau_{2D}\rangle)$ values from Fig. 1(a) were normalized with respect to the bulk value for each exponent p and are plotted in Fig. 2(a) as a function of well thickness a and p. A dashed black line marks the thickness at which $PF_{2D}\cdot(\tau_{CRTA}/\langle\tau_{2D}\rangle)$ is equal to the bulk value. For all p values investigated, this thickness is approximately 20 nm: For all thicknesses larger than 20 nm, $PF_{2D}\cdot(\tau_{CRTA}/\langle\tau_{2D}\rangle)$ falls *below* the bulk value. We assume here that the p value of the dominant scattering mechanism is the same for quantum wells and for bulk.

The minimum value of $PF_{2D}\cdot(\tau_{CRTA}/\langle\tau_{2D}\rangle)$ is marked by a solid black line in Fig. 2(a) as a function of p. For thicknesses below the minimum, $PF_{2D}\cdot(\tau_{CRTA}/\langle\tau_{2D}\rangle)$ increases monotonically with increasing confinement. Above the minimum, $PF_{2D}\cdot(\tau_{CRTA}/\langle\tau_{2D}\rangle)$ increases up to the bulk value. This increase is monotonic for p values below 0.2—for larger p values, slight oscillations giving rise to additional local minima and maxima are seen. The minimum value of $\frac{PF_{2D}\cdot(\tau_{CRTA}/\langle\tau_{2D}\rangle)}{PF_{3D}\cdot(\tau_{CRTA}/\langle\tau_{3D}\rangle)}$, shown as a function of p in the inset of Fig. 2(a), falls as low as 0.68 for $p=-0.8$, increasing up to 0.89 for $p=1.5$.

Similar calculations were executed to model the thermoelectric properties of circular nanowires. As with quantum wells, for each nanowire radius r, $PF_{1D}\cdot(\tau_{CRTA}/\langle\tau_{1D}\rangle)$ increases monotonically with p and for each p value, a non-monotonic size-dependence is found (Fig. S1(a)).[29] The

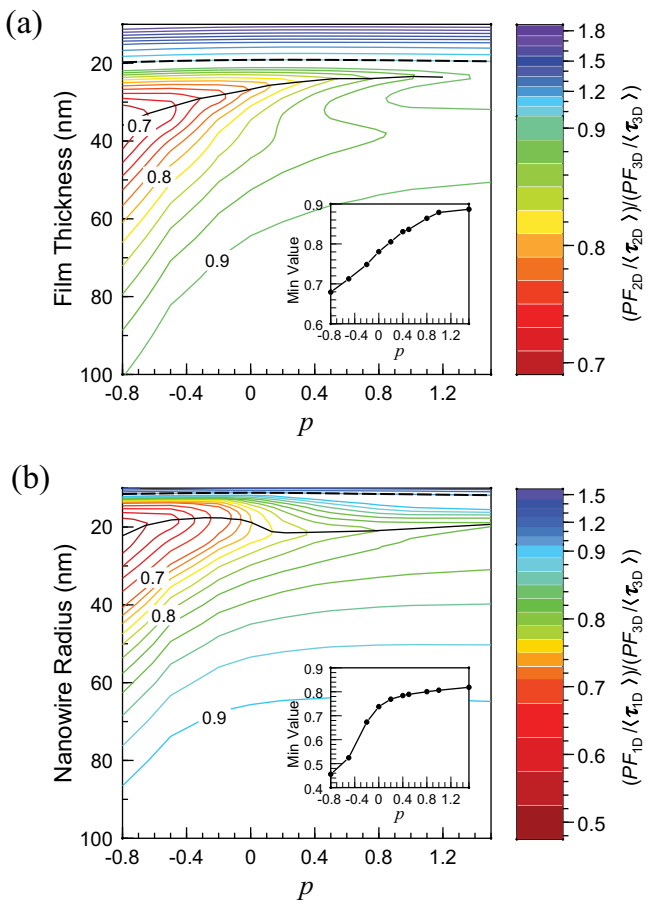

FIG. 2. (a) Bulk normalized $PF_{2D} \cdot (\tau_{CRTA}/\langle\tau_{2D}\rangle)$ as a function of p and film thickness a. The contour line of value 1, where $PF_{2D} \cdot (\tau_{CRTA}/\langle\tau_{2D}\rangle)$ equals the bulk value, is highlighted by the dashed black line. The solid black line traces the valley, and the inset shows this minimum value as a function of p. (b) Bulk normalized $PF_{1D} \cdot (\tau_{CRTA}/\langle\tau_{1D}\rangle)$ as a function of p and nanowire radius r. Dashed black line marks where $PF_{1D} \cdot (\tau_{CRTA}/\langle\tau_{1D}\rangle)$ equals the bulk value. The solid black line traces the valley and the inset shows this minimum value as a function of p. Note that in both (a) and (b) the vertical axis of the color scale bar is not scaled linearly.

optimized $PF_{1D} \cdot (\tau_{CRTA}/\langle\tau_{1D}\rangle)$ values for circular nanowires, normalized with respect to bulk, are shown in Fig. 2(b) as a function of r and p. The largest radius for which an improvement is seen over bulk falls between 11 and 12 nm for the entire range of p values (marked as dashed black line in Fig. 2(b)). The minimum in $PF_{1D} \cdot (\tau_{CRTA}/\langle\tau_{1D}\rangle)$, marked by a solid black line as a function of p, separates the size range in which $PF_{1D} \cdot (\tau_{CRTA}/\langle\tau_{1D}\rangle)$ increases with increasing confinement from the range in which $PF_{1D} \cdot (\tau_{CRTA}/\langle\tau_{1D}\rangle)$ increases with r up to the bulk value. For $p = 1.5$, the increase up to the bulk value is not monotonic, as slight oscillations can be seen between 19 and 30 nm (Fig. S1(b)).[29] The minimum value of $PF_{1D} \cdot (\tau_{CRTA}/\langle\tau_{1D}\rangle)$ relative to bulk is shown as a function of p in the inset of Fig. 2(b). The ratio $\frac{PF_{1D} \cdot (\tau_{CRTA}/\langle\tau_{1D}\rangle)}{PF_{3D} \cdot (\tau_{CRTA}/\langle\tau_{3D}\rangle)}$ falls as low as 0.46 (for $p = -0.8$), increasing up to 0.82 for $p = 1.5$.

The non-monotonic size-dependence of the thermoelectric power factor of quantum wells and nanowires has been previously explained in detail.[19] For small sizes, the system falls within the electric quantum limit. Only one subband is found within several k_BT of the Fermi energy and dominates transport. $PF \cdot (\tau_{CRTA}/\langle\tau\rangle)$ decreases as a^{-1} for quantum wells and r^{-2} for circular nanowires. For larger systems, additional subbands contribute to transport and $PF \cdot (\tau_{CRTA}/\langle\tau\rangle)$ increases with increasing size and electron density-of-states.

For film thicknesses above 31 nm and nanowire radii above 15 nm, $\frac{PF \cdot (\tau_{CRTA}/\langle\tau\rangle)}{PF_{3D} \cdot (\tau_{CRTA}/\langle\tau_{3D}\rangle)}$ increases monotonically with p. In this size range, confinement effects are weak, and $PF \cdot (\tau_{CRTA}/\langle\tau\rangle)$ falls below the bulk value. The monotonic increase in $\frac{PF \cdot (\tau_{CRTA}/\langle\tau\rangle)}{PF_{3D} \cdot (\tau_{CRTA}/\langle\tau_{3D}\rangle)}$ with increasing p is explained by an increase in the contribution of high-energy subbands. Transport is dominated by the subbands that fall within several k_BT of the Fermi energy. Through the energy-dependence of the scattering time, the electronic subbands are additionally weighted based on their energy relative to the conduction band edge. For a given size, as p increases the Fermi energy corresponding to the optimal power factor ($E_{f,max}$) increases from below the band edge into the band. This is because the states weighted with the largest τ value are those very close to the band edge for $p < 0$ and those far into the band for $p > 0$. With this increase in Fermi energy, additional subbands become close to $E_{f,max}$ and are relevant to transport. For a given size, the effective DOS becomes more bulk-like and $PF \cdot (\tau_{CRTA}/\langle\tau\rangle)$ increases up to the bulk value as p increases.

The secondary minima and maxima seen for large p values ($p > 0.2$ for quantum wells and $p > 1$ for nanowires) are attributed to the movement of subband energies across the Fermi energy as the size is varied. The effect is most substantial for large p values, for which high-energy subbands are given the most weight and $E_{f,max}$ is driven far into the band. For large p values, the optimal Fermi energy also oscillates with size, adjusting to the changing subband energies. On the other hand, for small p values, $E_{f,max}$ smoothly varies between its value in the electric quantum limit to its value in bulk (remaining close to the lowest subband). As a result, no oscillations are observed in $PF \cdot (\tau_{CRTA}/\langle\tau\rangle)$ (Fig. S2).[29]

Calculations were done for quantum wells in which two different scattering terms are present. The total scattering rate is given by

$$\tau^{-1} = \tau_1^{-1} + \tau_2^{-1} = \left(\frac{1}{C_1 \cdot (E/k_BT)^{p_1}} + \frac{1}{C_2 \cdot (E/k_BT)^{p_2}}\right), \tag{3}$$

where C_1 and C_2 are constant coefficients with units of time. The electron-energy dependence of the scattering times are shown in Fig. 3(a), where the energy is shown with respect to the conduction band edge, $p_1 = -0.5$ and $p_2 = 0.4$. The scattering time may decrease monotonically (e.g., for the case with $C_1/C_2 = 0$), increase monotonically (e.g., for the case with $C_1/C_2 = \infty$), or exhibit a maximum (e.g., for the case with $C_1/C_2 = 1$). The last case represents the most realistic scenario in which one scattering mechanism dominates for low-energy electrons and a second mechanism dominates for high-energy electrons.

The $PF_{2D} \cdot (\tau_{CRTA}/\langle\tau_{2D}\rangle)$ values are shown in Fig. 3(b) as a function of well thickness a for $p_1 = -0.5$, $p_2 = 0.4$ and various coefficient ratios C_1/C_2. For all thicknesses, $PF_{2D} \cdot (\tau_{CRTA}/\langle\tau_{2D}\rangle)$ moves monotonically between the two

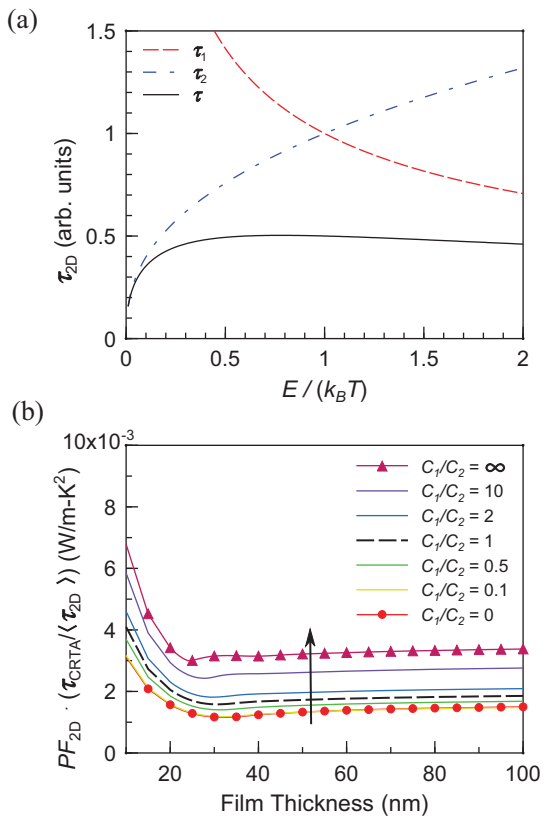

FIG. 3. (a) Scattering times $\tau_1 = C_1(E/k_BT)^{-0.5}$, $\tau_2 = C_2(E/k_BT)^{0.4}$, and the total $\tau = (\tau_1^{-1} + \tau_2^{-1})^{-1}$ as a function of carrier energy. (b) $PF_{2D} \cdot (\tau_{CRTA}/\langle\tau_{2D}\rangle)$ as a function of film thickness for $p_1 = -0.5$, $p_2 = 0.4$, and various ratios of coefficients C_1 and C_2. The black arrow indicates the trend of increasing C_1/C_2.

extreme cases: (1) $C_1/C_2 \to 0$, corresponding to a single scattering mechanism with $p = -0.5$, and (2) $C_1/C_2 \to \infty$, corresponding to a single scattering mechanism with $p = 0.4$. The qualitative behavior of the curves is similar to that for a single scattering mechanism. All curves exhibit a minimum, which shifts between 32 nm (for $C_1/C_2 \to 0$) and 25 nm (for $C_1/C_2 \to \infty$). For larger film thicknesses, $PF_{2D} \cdot (\tau_{CRTA}/\langle\tau_{2D}\rangle)$ increases up to the bulk value.

This work illustrates that the particular scattering model, whether the scattering time increases, decreases, or exhibits a maximum as a function of electron energy, does not affect the qualitative behavior of the thermoelectric power factor of nanostructures. Quantitatively, however, the magnitude of $PF \cdot (\tau_{CRTA}/\langle\tau\rangle)$ consistently increases with increasing p. We note that a scattering time function that increases with energy ($p > 0$) corresponds to a system in which the low-energy (cold) electrons are preferentially scattered over high-energy (hot) electrons. This "energy filtering" has long been recognized as a means for improving the thermoelectric performance.[10,11,30] In real systems, energy filtering can be achieved by energy-dependent scattering of electrons by grain boundaries. Increases in the power factor via energy filtering have been demonstrated in InGaAs/InGaAlAs superlattices[4] and Pb/PbTe nanocomposites.[5] The results of this work also indicate that the thermoelectric power factor has a stronger dependence on p than on system size (a and r). For systems with a low effective p value, size reduction may be counterproductive as the nanostructure power factor may fall approximately 50% below the bulk value.

In summary, we have reported a non-monotonic size-dependence in the thermoelectric power factor ($PF \cdot (\tau_{CRTA}/\langle\tau\rangle)$) of quantum wells and nanowires for an arbitrary energy-dependent scattering time of the form $\tau = C \cdot (E/k_BT)^p$. Regardless of the value of exponent p, the $PF \cdot (\tau_{CRTA}/\langle\tau\rangle)$ falls below the bulk value for most of the size range investigated (for $a > 20$ nm, $r > 12$ nm). Due to the increasing contribution of high-energy electrons, an increase in p leads to a monotonic increase in (a) the $PF \cdot (\tau_{CRTA}/\langle\tau\rangle)$ for a specific system size as well as for bulk and (b) the minimum value of $\frac{PF \cdot (\tau_{CRTA}/\langle\tau\rangle)}{PF_{3D} \cdot (\tau_{CRTA}/\langle\tau_{3D}\rangle)}$.

[1]G. Joshi, H. Lee, Y. Lan, X. Wang, G. Zhu, D. Wang, R. W. Gould, D. C. Cuff, M. Y. Tang, M. S. Dresselhaus, G. Chen, and Z. Ren, Nano Lett. **8**, 4670 (2008).
[2]B. Poudel, Q. Hao, Y. Ma, Y. Lan, A. Minnich, B. Yu, X. Yan, D. Wang, A. Muto, D. Vashaee, X. Chen, J. Liu, M. S. Dresselhaus, G. Chen, and Z. Ren, Science **320**, 634 (2008).
[3]A. I. Hochbaum, R. Chen, R. D. Delgado, W. Liang, E. C. Garnett, M. Najarian, A. Majumdar, and P. Yang, Nature **451**, 163 (2008).
[4]J. M. O. Zide, D. Vashaee, Z. X. Bian, G. Zeng, J. E. Bowers, A. Shakouri, and A. C. Gossard, Phys. Rev. B **74**, 205335 (2006).
[5]J. P. Heremans, C. M. Thrush, and D. T. Morelli, J. Appl. Phys. **98**, 063703 (2005).
[6]J. P. Heremans, V. Jovovic, E. S. Toberer, A. Saramat, K. Kurosaki, A. Charoenphakdee, S. Yamanaka, and G. J. Snyder, Science **321**, 554 (2008).
[7]C. M. Jaworski, V. Kulbachinskii, and J. P. Heremans, Phys. Rev. B **80**, 233201 (2009).
[8]O. Rabin, Y.-M. Lin, and M. S. Dresselhaus, Appl. Phys. Lett. **79**, 81 (2001).
[9]T. Koga, X. Sun, S. B. Cronin, and M. S. Dresselhaus, Appl. Phys. Lett. **73**, 2950 (1998).
[10]A. J. Minnich, M. S. Dresselhaus, Z. F. Ren, and G. Chen, Energy Env. Sci. **2**, 466 (2009).
[11]C. J. Vineis, A. Shakouri, A. Majumdar, and M. G. Kanatzidis, Adv. Mater. **22**, 3970 (2010).
[12]L. D. Hicks and M. S. Dresselhaus, Phys. Rev. B **47**, 16631 (1993).
[13]L. D. Hicks and M. S. Dresselhaus, Phys. Rev. B **47**, 12727 (1993).
[14]N. Mingo, Appl. Phys. Lett. **84**, 2652 (2004).
[15]N. Mingo, Appl. Phys. Lett. **85**, 5986 (2004).
[16]D. A. Broido and T. L. Reinecke, Phys. Rev. B **64**, 045324 (2001).
[17]D. A. Broido and T. L. Reinecke, Appl. Phys. Lett. **77**, 705 (2000).
[18]D. A. Broido and T. L. Reinecke, Appl. Phys. Lett. **70**, 2834 (1997).
[19]J. E. Cornett and O. Rabin, Appl. Phys. Lett. **98**, 182104 (2011).
[20]J. E. Cornett and O. Rabin, Phys. Rev. B **84**, 205410 (2011).
[21]Y.-M. Lin, M. Sc. thesis, Massachusetts Institute of Technology, 2000.
[22]N. W. Ashcroft and N. D. Mermin, *Solid State Physics* (Holt, Rinehart and Winston, New York, 1976).
[23]J. Zhou, R. Yang, G. Chen, and M. S. Dresselhaus, Phys. Rev. Lett. **107**, 226601 (2011).
[24]V. I. i. Fistul, *Heavily Doped Semiconductors* (Plenum, 1969).
[25]D. Chattopadhyay and H. J. Queisser, Rev. Mod. Phys. **53**, 745 (1981).
[26]W. Zawadzki and W. Szymanska, J. Phys. Chem. Solids **32**, 1151 (1971).
[27]R. A. Stradling and R. A. Wood, J. Phys. C: Solid State Phys. **3**, L94 (1970).
[28]O. Madelung, *Semiconductors: Group IV Elements and III-V Compounds* (Springer-Verlag, 1991).
[29]See supplementary material at http://dx.doi.org/10.1063/1.4729381 for calculated $PF_{1D} \cdot (\tau_{CRTA}/\langle\tau_{1D}\rangle)$ values (Fig. S1) and a plot of $E_{f,max}$ and the first 7 subband energies as a function of film thickness (Fig. S2).
[30]D. Vashaee and A. Shakouri, J. Appl. Phys. **95**, 1233 (2004).